NANO LETTERS

2008
Vol. 8, No. 7
2106-2111

Optical Response of Strongly Coupled Quantum Dot−Metal Nanoparticle Systems: Double Peaked Fano Structure and Bistability

Ryan D. Artuso*,† and Garnett W. Bryant‡

Joint Quantum Institute and Department of Physics, University of Maryland, College Park, Maryland 20742-4111, and Joint Quantum Institute and Atomic Physics Division, National Institute of Standards and Technology, Gaithersburg, Maryland 20899-8423

Received April 1, 2008

ABSTRACT

In this communication, we study the optical response of a semiconductor quantum dot (SQD) coupled with a metal nanoparticle (MNP). In particular, we explore the relationship between the size of the constituents and the response of the system. We identify, here, three distinct regimes of behavior in the strong field limit that each exhibit novel properties. In the first regime, we find that the energy absorption spectrum displays an asymmetrical Fano shape (as previously predicted). It occurs when there is interference between the applied field and the induced field produced by the SQD at the MNP. When the coupling is increased by increasing the size of the SQD, we find a double peaked Fano structure in the response. This second peak occurs when the induced field becomes stronger than the external field. As the coupling is further increased by increasing the sizes of both the SQD and the MNP, we find a regime of bistability. This originates when the self-interaction of the SQD becomes significant. We explore these three regimes in detail and set bounds on each.

I. Introduction. Advances in nanoscience have allowed for the construction of nanosuperstructures. By using various combinations of the available building blocks (nanowires, semiconductor quantum dots, metal nanoparticles, biolinkers, etc.) to create these superstructures, novel physical phenomena may be explored. Such structures will allow the study of physics at the interface of classical and quantum mechanics and could provide the technology for a number of devices in the field of quantum information. These structures should allow for the physical transportation of excitations as well as the transportation of coherent states. Experiments have already demonstrated the plausibility of creating and studying such superstructures. Exciting results have been attained, such as the transportation of entangled photons by surface plasmons,[1] the polarization selective enhancement of quantum dot photoluminescence when coupled to metal nanoparticles,[2] and centimeter scale propagation of entangled plasmons,[3,4] as well as the creation of a single plasmon in a temporal state of superposition.[3] Recently, hybrid structures consisting of a quantum dot and a metal nanoparticle joined by a biolinker have been assembled and studied.[5] Furthermore, the radiative coupling of a CdSe quantum dot to a silver nanowire has been explored.[6,7]

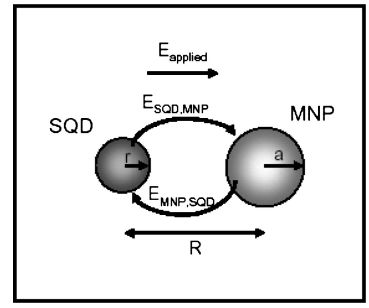

Figure 1. An applied field induces a polarization in both the MNP and the SQD which in turn allows for a dipole−dipole coupling.

We discuss here the response of a hybrid nanostructure molecule consisting of a semiconductor quantum dot (SQD) and a metal nanoparticle (MNP) subject to an applied electric field. This system has been studied in ref 8, in ref 9 with multiple metal nanoparticles, and similarly in ref 10 with a nanowire replacing the spherical MNP. Similarly, the dipole−dipole coupling between two fluorescent molecules mediated by a chain of silver nanoparticles has also been studied.[11]

* Corresponding author. E-mail: artuso@umd.edu.
† University of Maryland.
‡ National Institute of Standards and Technology.

10.1021/nl800921z CCC: $40.75
Published on Web 06/18/2008

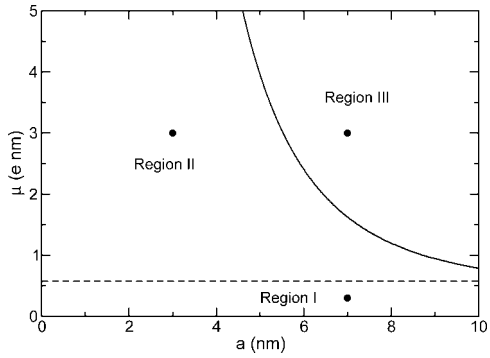

Figure 2. μ vs a phase diagram for $R = 13$ nm in the strong field limit. Points denote locations pictured in Figures 3, 4, 6, and 7.

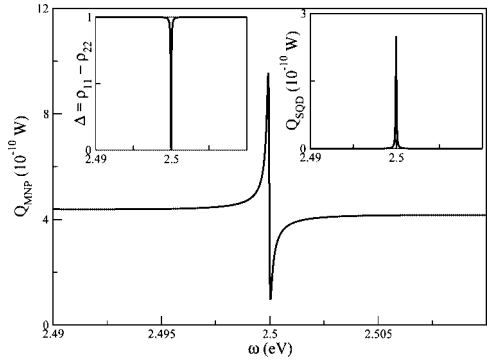

Figure 3. Region I. Power absorption density of the MNP with $R = 13$ nm, $a = 7$ nm, and $\mu = 0.3$ e nm. Left inset shows a population difference of 0 at resonance. Right inset shows a sharp response in the SQD.

The excitations of the SQD are discrete excitons. The plasmonic excitations of the MNP provide a strong continuous spectral response. There is no direct tunneling between the MNP and the SQD. However, because of the long-range Coulomb interaction, there is a dipole−dipole interaction that will allow them to couple and that leads to excitation transfer. The sharp optical response of the excitons coupled with the strong optical response of the plasmons will allow for the appearance of exotic hybrid states and signatures for the optical response.

Previously, the weak field limits (driving field of 1W/cm^2) were studied. A shift and broadening of the peak in the energy absorption spectrum due to the coupling between the exciton in the SQD and the plasmon in the MNP was found.[8] In the strong field limit, when the SQD and MNP are weakly coupled, an asymmetrical Fano shape develops in the energy absorption spectrum (also found in ref 8).

In this communication, we probe further the strong applied field limit. We find that the behavior is much more complex than previously determined. In addition to the regime for weak coupling, we find two new regimes of behavior for strong coupling. As the SQD is increased in size (thus the strength of the coupling is increased), we find a modification to the asymmetrical Fano effect with the appearance of an additional peak. This peak brings with it two nodes in the response that replace the typical minimum associated with the Fano effect. When the MNP and SQD are increased in size, we find an extreme broadening of the modified Fano shape that washes out the second peak. More interestingly, we find that the response is nonlinear in this third regime. This nonlinearity is due to the significant self-interaction of the SQD (feedback through the MNP). In this regime, we find the existence of multiple steady state solutions leading to a bistability with one of the stable solutions having a discontinuous energy spectrum.

In section II, we discuss the system in full detail as well as calculate the response of the MNP. In section III, we identify and discuss the three regimes of behavior for the strong field case as well as examine the polarization dependent effects. In section IV, we present our conclusions.

II. Setup. As in ref 8, we consider a spherical SQD with radius r interacting with a spherical MNP of radius a, separated by a distance R (as shown in Figure 1). The entire system is subject to an applied electric field $E = E_0 \cos(\omega t)$. We assume that all distances are small enough that retardation effects can be ignored. We treat the SQD quantum mechanically in the density matrix formalism with exciton energy $\hbar\omega_0$, dipole moment μ, and dielectric constant ε_S. In the dipole limit, only the three bright excitons (one for each optical axis) participate in the interaction. Dark excitons do contribute to the exciton lifetime, however. We treat the MNP as a classical spherical dielectric particle with dielectric function $\varepsilon_M(\omega)$.

The Hamiltonian for the SQD, H_{SQD}, is

$$H_{SQD} = \hbar\omega_0 \hat{a}^\dagger \hat{a} - \mu E_{SQD} \hat{a} - \mu E^*_{SQD} \hat{a}^\dagger \tag{1}$$

where $\hat{a}$ and $\hat{a}^\dagger$ are the exciton annihilation and creation operators. E_{SQD} is the total electric field felt by the SQD and consists of the applied, external field, E, and the induced, internal field, produced by the polarization of the MNP, $E_{MNP,\,SQD}$

$$E_{SQD} = E + \frac{1}{4\pi\varepsilon_0} \frac{s_\alpha P_{MNP}}{\varepsilon_{effM} R^3} \tag{2}$$

where $\varepsilon_{effM} = [2\varepsilon_0 + \varepsilon_M(\omega)]/3\varepsilon_0$, and $s_\alpha = 2$ (-1) when the applied field is parallel (perpendicular) to the major axis of the system. The polarization of the MNP is (see ref 12),

$$P_{MNP} = (4\pi\varepsilon_0)\gamma a^3 \left(E + \frac{1}{4\pi\varepsilon_0} \frac{s_\alpha P_{SQD}}{\varepsilon_{effS} R^3} \right) \tag{3}$$

where $\varepsilon_{effS} = [2\varepsilon_0 + \varepsilon_S]/3\varepsilon_0$ and $\gamma = [\varepsilon_M(\omega) - \varepsilon_0]/[2\varepsilon_0 + \varepsilon_M(\omega)]$. Making use of the density matrix ρ to calculate the polarization of the SQD, we take the ensemble average of the dipole moment. We then have $P_{SQD} = \mu(\rho_{12} + \rho_{21})$ (see ref 13). Putting this in E_{SQD}, we have

$$E_{SQD} = \frac{2\hbar}{\mu E_0} E\Omega + \frac{\hbar}{\mu} G(\rho_{12} + \rho_{21}) \tag{4}$$

where we have defined

$$G = \frac{s_\alpha^2 \gamma a^3 \mu^2}{4\pi\varepsilon_0 \varepsilon_{effM} \varepsilon_{effS} \hbar R^6}$$

$$\Omega = \frac{E_0 \mu}{2\hbar} \left(1 + \frac{\gamma a^3 s_\alpha}{\varepsilon_{effM} R^3} \right)$$

G arises when the applied field polarizes the SQD, which in turn polarizes the MNP and then produces a field to interact

with the SQD. Thus, this can be thought of as the self-interaction of the SQD because this coupling to the SQD depends on the polarization of the SQD. The first term in Ω is just the direct coupling to the applied field, and the second term is the field from the MNP that is induced by the applied field.

We solve the master equation

$$\dot{\rho} = \frac{i}{\hbar}[\rho, H_{SQD}] - \Gamma(\rho) \tag{5}$$

where $\Gamma(\rho)$ is the relaxation matrix with entries $\Gamma_{11} = (\rho_{11} - 1)/\tau_0$, $\Gamma_{12} = \Gamma_{21}^* = \rho_{12}/T_{20}$ and $\Gamma_{22} = \rho_{22}/\tau_0$. The relaxation time τ_0 contains a contribution from nonradiative decay to dark states. Factoring out the high frequency part of the off-diagonal terms of the density matrix, we write

$$\rho_{12} = (A + iB)e^{i\omega t}$$
$$\rho_{21} = (A - iB)e^{-i\omega t}$$
$$\Delta = \rho_{11} - \rho_{22}$$

Making use of these definitions and the rotating wave approximation, we arrive at a set of coupled, nonlinear differential equations.

$$\begin{aligned}
\dot{A} &= -\frac{A}{T_{20}} + (\omega - \omega_0)B + (\Omega_I + G_I A + G_R B)\Delta \\
\dot{B} &= -\frac{B}{T_{20}} - (\omega - \omega_0)A - (\Omega_R + G_R A - G_I B)\Delta \\
\dot{\Delta} &= \frac{1 - \Delta}{\tau_0} - 4\Omega_I A + 4\Omega_R B - 4G_I(A^2 + B^2)
\end{aligned} \tag{6}$$

In the steady state limit, we set the left-hand side of eq 6 to zero. Because of the nonlinear nature of these equations, more than one steady state solution can exist for certain values of the parameters. In these regions, we must solve the full set of dynamical equations, allowing them to evolve from the initial conditions for times on the order of 10 ns to reach the steady state. This allows us to identify the dependence of the steady state on the starting conditions. Evolution for 10 ns was sufficient to reach steady state in all cases we considered.

A. Energy. The rate at which energy is absorbed by our system consists of two parts, Q_{SQD} and Q_{MNP}. The SQD absorbs energy by the creation of an exciton. The rate is just $Q_{SQD} = \hbar\omega_0\rho_{22}/\tau_0$. To calculate the energy absorbed by the MNP, we take the time average of the volume integral, $\int j \cdot E \, dv$. The electric field felt by the MNP is the applied field plus the field due to the polarization of the SQD,

$$\begin{aligned}
E_{MNP} &= E + \frac{1}{4\pi\varepsilon_0}\frac{s_\alpha \mu}{\varepsilon_{effS} R^3}(\rho_{12} + \rho_{21}) \\
&= \left(E_0 + \frac{s_\alpha \mu A}{2\pi\varepsilon_0 \varepsilon_{effS} R^3}\right)\cos(\omega t) + i\frac{s_\alpha \mu B}{2\pi\varepsilon_0 \varepsilon_{effS} R^3}\sin(\omega t) \\
&= E_C \cos(\omega t) + iE_S \sin(\omega t)
\end{aligned} \tag{7}$$

where

$$E_C = E_0 + \frac{s_\alpha \mu}{2\pi\varepsilon_0 \varepsilon_{effS} R^3} A$$

is the component of the field that is in phase with the applied field and

$$E_S = \frac{s_\alpha \mu}{2\pi\varepsilon_0 \varepsilon_{effS} R^3} B$$

is 90° out of phase with the applied field.

We calculate the current in the MNP from the derivative of P_{MNP}. Making use of eq 7, we find Q_{MNP} to be

$$\begin{aligned}
Q_{MNP} &= 2\pi\varepsilon_0 \omega a^3 Im(\gamma)\left\{\left(E_0 + \frac{s_\alpha \mu A}{2\pi\varepsilon_0 \varepsilon_{effS} R^3}\right)^2 + \left(\frac{s_\alpha \mu B}{2\pi\varepsilon_0 \varepsilon_{effS} R^3}\right)^2\right\} \\
&= 2\pi\varepsilon_0 \omega a^3 Im(\gamma)\{E_C{}^2 + E_S{}^2\}
\end{aligned} \tag{8}$$

Thus, E_C and E_S are key in determining the shape of the response. Since E_S is out of phase with the applied field, it will typically be substantially smaller than E_C. However, for the strongest coupling that we will look at, E_C and E_S are comparable.

III. Analysis of μ Versus a Parameter Space in the Large Field Limit. In this paper, we will consider the large field limit as defined in ref 8 (intensity of 10^3 W/cm^2) with E parallel to the axis of our SQD−MNP molecule; that is, $s_\alpha = 2$. In this limit, most of the energy absorbed by the system will be due to the MNP, so our focus will be on the field felt by MNP.

For numerical calculations, we take $\varepsilon_M(\omega)$ as the bulk dielectric constant of gold as found experimentally.[14] For the SQD, we take $\varepsilon_S = 6\varepsilon_0$ and the exciton resonant frequency to be 2.5 eV which is near the broad plasmon frequency of gold (peak near 2.4 eV with a width of approximately 0.25 eV). For the relaxation times of the SQD, we take $\tau_0 = 0.8$ ns and $T_{20} = 0.3$ ns. For the MNP size regime we consider, the plasmon resonance for a sphere varies little with particle size. However, the SQD exciton resonance depends strongly on size in small SQDs. In this paper, we consider the simplest model and ignore the size dependence of the exciton energy. While this is clearly an oversimplification, it allows us to identify the range of optical signatures which are possible in the strong-field limit.

By manipulating a and μ, effectively, the sizes of the MNP and SQD, respectively, we can control the strengths of the three different couplings (G and the two terms that make up Ω). Looking at the solutions to the differential equations, both dynamically and in the steady state limit, we find three distinct regions in the a versus μ parameter space (see Figure 2).

In region I, response to the driving field is dominant as previously discussed,[8] although interference between the driving field and the induced field can produce a Fano interference. For stronger couplings (regions II and III) new structure in the response emerges and bistability induced by the self-interaction becomes important. We discuss each region in turn.

A. Region I: Nonlinear Fano Effect. The first region is the regime of weak coupling between the SQD and the MNP discussed extensively in ref 8. At low driving fields, the peak response broadens and shifts because of the exciton−plasmon coupling. At strong fields, the energy absorption spectrum displays an asymmetrical Fano shape (see Figure 3). It occurs

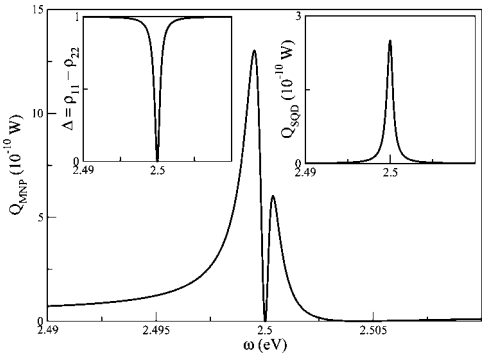

Figure 4. Region II. Power absorption density of the MNP with $R = 13$ nm, $a = 3$ nm, and $\mu = 3$ e nm. Left inset shows a population difference of 0 at resonance. Right inset shows a broadening of the response in the SQD.

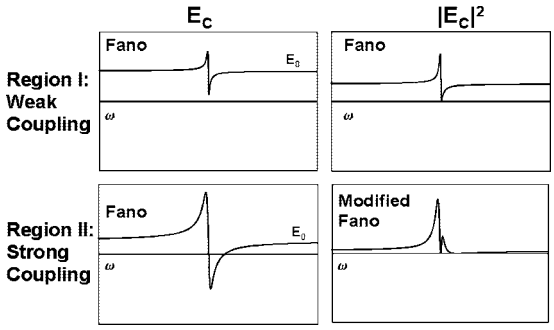

Figure 5. Emergence of the modified Fano shape is due to E_C crossing zero. This occurs when the internal field can be larger than the external field.

when there is interference between the applied field and the internal field produced by the SQD at the MNP. In this region, the dominant component of the field on the MNP is E_C, with E_S being negligible at weak coupling. More importantly, E_C is dominated by the applied field E.

B. Region II: Modified Fano Effect−Double Peak Structure. When the coupling is increased by increasing μ, the character of the Fano response becomes more complicated. Region II is characterized by the additional peak that appears in the Fano line shape of region I (see Figure 4). This second peak occurs where E_C reverses sign (in this region of parameter space, E_S is still an order of magnitude smaller; see Figure 5). For this to happen, the internal field, $[s_\alpha \mu / 2\pi\varepsilon_0\varepsilon_{effS}R^3]A$, must be larger than the external field, E_0, over a range of frequencies. When E_C changes sign, this yields two locations where the field on the MNP is nearly completely canceled and the metal becomes reflective. The absorption remains finite only because the small out-of-phase component E_S is nonzero.

By setting $E_C = 0$, we find the line separating region I from region II to be

$$\mu(a) = -\frac{2\pi\varepsilon_0\varepsilon_{effS}R^3E_0}{s_\alpha A} \tag{9}$$

A varies with a slowly over the parameter space and thus $\mu(a)$ is approximately constant. At the frequency where this double peak occurs, A has a typical value of -0.15. Using this value for A, we find this line to be approximately $\mu = 0.59$ e nm. Fitting to our data, we find this line to be $\mu(a) = 0.574$ e nm plus a small exponential term (negligible for $a < 10$ nm). Note that in ref 8 the value of μ that was used in numerical calculations was 0.65 e nm, which falls nearly on this boundary.

When we let μ and a vary in such a way as to approach region I from region II, this second peak decreases in size. Similarly, the farther away from region I we get into region II, the larger this second peak becomes. The transition between these two regions is smooth; that is, the extra peak vanishes at the transition boundary (see Figure 5).

C. Region III: Bistability. When the coupling is increased further by increasing μ and a, a region of bistable response emerges (region III). In this limit, the field that is produced by the SQD and then reflected off the MNP and back onto the SQD (the self-interaction of the SQD) is sufficiently strong to induce a significant contribution to the out of phase component of the density matrix, B, and thus E_S. Thus, there is a non-negligible Q_{MNP}, even when $E_C = 0$. This, along with a general broadening due to the increased field strength, can cause the double peak structure to disappear (see Figure 6).

Region III is characterized by a bistability in the steady state solutions. Given identical values μ and a, different initial conditions lead to different steady states (see Figures 6 and 7). This bistability only exists near the resonance frequency of the SQD; away from resonance, all initial conditions lead to identical steady states. For $R = 13$ nm, $a = 7$ nm, and $\mu = 3$ e nm, the width of bistability is on the order of 0.2 meV with the initial conditions ($A(0) = 0$, $B(0) = 0$, $\Delta(0) = 0$; see Figure 7). As the values of a and μ get closer to region II, this window in ω space shrinks.

Outside the frequency window of this nonlinear behavior, the steady state equations, which are of third order in Δ, give one real physical solution and two complex solutions. Inside this window, all three solutions are real, and we must work with the full differential equations to explore the dynamics.

This region is defined by the relative strengths of G and Ω. From eq 6, we see that G is the part of the electric field

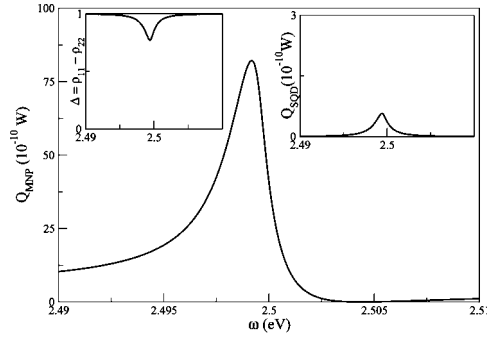

Figure 6. Region III. Power absorption density of the MNP with $R = 13$ nm, $a = 7$ nm, $\mu = 3$ e nm, and the initial conditions $A(0) = 0$, $B(0) = 0$, and $\Delta(0) = 1$. Left inset shows a population difference of about 0.8 at resonance. Right inset shows the very broad and weak response of the SQD.

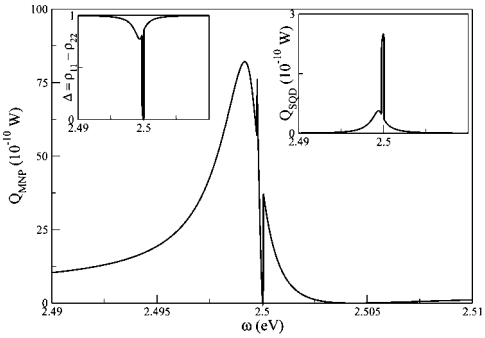

Figure 7. Region III. Power absorption density of the MNP with $R = 13$ nm, $a = 7$ nm, $\mu = 3$ e nm, and the initial conditions $A(0) = 0$, $B(0) = 0$, and $\Delta(0) = 0$. The bistability causes discontinuities in the responses of the MNP, the SQD, and the population difference.

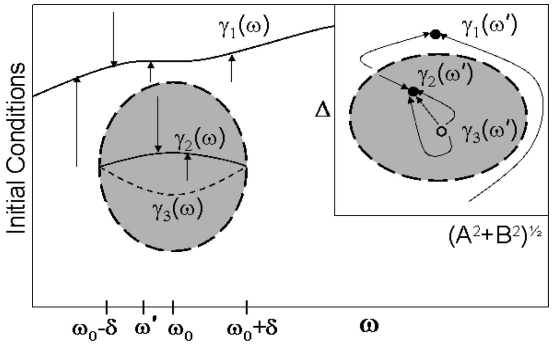

Figure 8. Schematic representation of initial conditions vs frequency. γ_1 represents the continuous steady state; γ_2 represents the discontinuous steady state, and γ_3 represents unstable steady state. Note that γ_2 and γ_3 only exist inside the frequency interval $(\omega_0 - \delta, \omega_0 + \delta)$. Arrows show how particular initial conditions evolve to one of the three solutions. Inset shows a cross section in ω space. Points arbitrarily close to γ_3 evolve to γ_2.

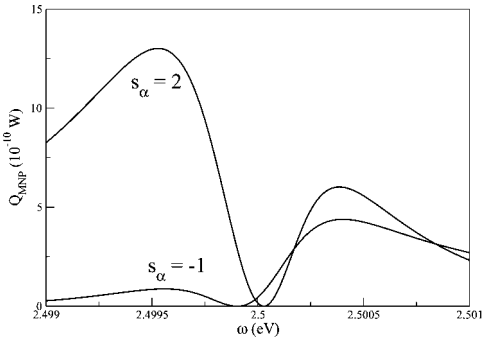

Figure 9. Effect of polarization on the response of the MNP in region II ($R = 13$ nm, $a = 3$ nm, and $\mu = 3$ e nm). Curve labeled $s_\alpha = 2$ is for the applied field parallel to the main axis of the molecule; $s_\alpha = -1$ is for perpendicular polarization.

that describes the feedback because it is linear in the density matrix elements. For $\Omega/G \approx 1$, we see that

$$\mu(a) = 2\pi\varepsilon_0 E_0 \left(\frac{\varepsilon_{effM}\varepsilon_{effS}}{s_\alpha^2 \gamma} \frac{R^6}{a^3} + \frac{\varepsilon_{effS}}{s_\alpha} R^3 \right) \tag{10}$$

Putting in typical values for ε_{effM}, ε_{effS}, and γ and taking the magnitude of the first term, we get the following approximation

$$\mu(a) = 0.22 \frac{E_0 R^6}{a^3} + 0.46 E_0 R^3$$

Our fitting puts the line at

$$\mu(a) = 1.10 \frac{E_0 R^6}{a^3} + 1.54 E_0 R^3 \tag{11}$$

We see that bistability occurs once G becomes a significant factor when compared with Ω. When E_0 and R increase, this region shrinks and this bistable state eventually becomes physically inaccessible. It would appear that the easiest way to find this region of bistability is when E_0 becomes small in the weak field limit. However, in this limit, we found that, while most choices of a and μ lead to a bistability, the frequency width of the bistability is negligible making this feature experimentally inaccessible. Thus, this bistable state is only acccessable in the regime that we have discussed here.

As we approach the boundary between region II and region III starting from inside region II, the width of the second peak, in the modified Fano shape, decreases while the magnitude remains. At the boundary, this peak becomes pinched with negligible width for one of the steady state solutions resulting in the discontinuous jump evident in Figure 7. This transition is not smooth due to the nonlinear nature of region III.

1. Analysis of Initial Conditions. In the region of bistability (both in a vs μ space and in ω space), there are three solutions. One of these three solutions, γ_1, is smooth and continuous as a function of ω and displays a very broad asymmetrical Fano shape (see Figure 6). In this steady state, the dot is in the ground state ($\rho_{11} = 1$) when away from resonance and only weakly excited near resonance. The second solution, γ_2, is the same broad asymmetrical Fano shape away from resonance with a discontinuous jump near resonance in the energy absorption spectrum (see Figure 7). In this steady state, the dot becomes strongly excited near resonance ($\rho_{11} \approx \rho_{22} \approx {}^1/_2$). The third solution, γ_3, turns out to be unstable (initial conditions arbitrarily close to this point evolve to a different steady state).

The space of initial conditions can be divided into two regions, one for each of the two possible, stable, steady-state solutions. For a particular choice of parameters ($R = 13$ nm, $a = 7$ nm, $\mu = 3.5$ e nm) the region with the discontinuous solution is an ellipsoid centered at $A(0) = 0$, $B(0) = 0$, $\Delta(0) = 0$ and is found through numerical calculations to be approximately given by the relation

$$4(A(0)^2 + B(0)^2) + \Delta(0)^2 \leq 0.07 \tag{12}$$

with the region outside this ellipsoid having the smooth solution. The unstable solution is a line through this space parametrized by ω in the interval $(\omega_0 - \delta, \omega + \delta)$. It can begin inside or outside of the region given by, but near resonance is always inside for cases for which we looked (see Figure 8). For initial conditions exactly on this line, the state remains unchanged as it evolves in time. All other inital states evolve to γ_1 or γ_2.

As the initial conditions get close to the boundary of this region, the width ($\delta\omega = 2\delta$) shrinks. Numerically, we have

found the relationship between the initial conditions and this width to be approximately

$$[4(A(0)^2 + B(0)^2) + \Delta(0)^2]^2 + \left(\frac{\delta\omega}{4\times10^{-3}\text{eV}}\right)^2 = 0.005$$

D. Polarization. So far, we have taken the applied field parallel to the major axis of the MNP−SQD system ($s_\alpha = 2$). There are two effects when the polarization is perpendicular to the main axis. First, the shape of the Fano structures is reversed (see Figure 9). For parallel polarization with the induced dipoles of the SQD and MNP aligned end-to-end, the response is enhanced below resonance. For perpendicular polarization with the induced dipoles aligned side-by-side, the response is enhanced above resonance. This accounts for the shape reversal. Second, is the shift upward of the boundaries of regions I, II, and III, as described by equations 9 and 10, by a factor of 2 to 4 (note in eq 9, A also reverses sign with s_α). The boundaries are defined by the relative magnitudes of the direct coupling, the induced field and the self-interaction. These relative magnitudes are different for the two polarizations. This results in the existence of points in parameter space that change from one region to another when the polarization is switched.

IV. Concluding Remarks. To summarize, we have investigated the optical response of a semiconductor quantum dot coupled with a metal nanoparticle. We have probed the strong applied electric field limit by treating the SQD quantum mechanically in the density matrix formalism and the MNP as a classical spherical dielectric. The behavior of this system is highly dependent on the relative sizes of the MNP and SQD. There are three distinct regimes of behavior in the strong field limit. Each exhibits novel properties. By varying the sizes of the metal nanoparticle and the quantum dot, we were able to set bounds on each of these regions. In the region of weak coupling, we find the energy absorption spectrum displays an asymmetrical Fano shape as previously predicted. It occurs when there is interference between the applied field and the internal field produced by the SQD at the MNP. In the strong coupling regime, we find that the behavior is more complex. When the coupling is increased by increasing the size of the SQD, we find a doubled peaked Fano structure in the response. This second peak occurs where the internal field becomes stronger than the external field. As the coupling is further increased by increasing the sizes of both the SQD and the MNP, the self-interaction of the SQD becomes significant. Here, we find a regime of bistability in which states with different initial conditions evolve to different steady states.

References

(1) Altewischer, E.; van Exter, M. P.; Woerdman, J. P. Plasmon-assisted transmission of entangled photons. *Nature* **2002**, *418* (6895)), 304–306.

(2) Mertens, H.; Biteen, J. S.; Atwater, H. A.; Polman, A. Polarization-selective plasmon-enhanced silicon quantum-dot luminescence. *Nano Lett.* **2006**, *6* (11)), 2622–2625.

(3) Griffin, P F; Weatherill, K J; MacLeod, S G; Potvliege, R M; Adams, C. S. Spatially selective loading of an optical lattice by light-shift engineering using an auxiliary laser field. *New J. Phys.* **2006**, *8* (1)), 11.

(4) Sylvain, Fasel; Franck, Robin; Esteban, Moreno; Daniel, Erni; Nicolas, Gisin; Hugo, Zbinden. Energy-time entanglement preservation in plasmon-assisted light transmission. *Phys. Rev. Lett.* **2005**, *94* (11)), 110501.

(5) Pons, T.; Medintz, I. L.; Sapsford, K. E.; Higashiya, S.; Grimes, A. F.; English, D. S.; Mattoussi, H. On the quenching of semiconductor quantum dot photoluminescence by proximal gold nanoparticles. *Nano Lett.* **2007**, *7* (10)), 3157–3164.

(6) Akimov, A. V.; Mukherjee, A.; Yu, C. L.; Chang, D. E.; Zibrov, A. S.; Hemmer, P. R.; Park, H.; Lukin, M. D. Generation of single optical plasmons in metallic nanowires coupled to quantum dots. *Nature* **2007**, *450* (7168)), 402–406.

(7) Fedutik, Y.; Temnov, V. V.; Schops, O.; Woggon, U.; Artemyev, M. V. Exciton-plasmon-photon conversion in plasmonic nanostructures. *Phys. Rev. Lett.* **2007**, *99* (13)), 136802.

(8) Zhang, Wei; Govorov, Alexander O.; Bryant, Garnett W. Semiconductor-metal nanoparticle molecules: Hybrid excitons and the nonlinear fano effect. *Phys. Rev. Lett.* **2006**, *97* (14)), 146804.

(9) Govorov, A. O.; Bryant, G. W.; Zhang, W.; Skeini, T.; Lee, J.; Kotov, N. A.; Slocik, J. M.; Naik, R. R. Exciton-plasmon interaction and hybrid excitons in semiconductor-metal nanoparticle assemblies. *Nano Lett.* **2006**, *6* (5)), 984–994.

(10) Cheng, Mu-Tian; Liu, Shao-Ding; Zhou, Hui-Jun; Hao, Zhong-Hua; Wang, Qu-Quan. Coherent excitonplasmon interaction in the hybrid semiconductor quantum dot and metal nanoparticle complex. *Opt. Lett.* **2007**, *32* (15)), 2125–2127.

(11) Lindberg, J.; Lindfors, K.; Seẗ al̈ a, T.; Kaivola, M. Dipole-dipole interaction between molecules mediated by a chain of silver nanoparticles. *J. Opt. Soc. Am. A* **2007**, *24* (11)), 3427–3431.

(12) Landau, L. D.; Lifshitz, E. M.; Pitaevskii L. P. *Electrodynamics of Continuous Media*; Butterworth-Heinemann Ltd: Oxford, 1984.

(13) Yariv A. *Quantum Electronics*; John Wiley and Sons: New York, 1975.

(14) Johnson, P. B.; Christy, R. W. Optical constants of the noble metals. *Phys. Rev. B* **1972**, *6* (12)), 4370–4379.

NL800921Z